JOURNAL OF
APPLIED
CRYSTALLOGRAPHY

Volume 52 (2019)

Supporting information for article:

Shape-fitting analyses of two-dimensional X-ray diffraction spots for strain-distribution evaluation in a β-$FeSi_2$ nanofilm

Shohei Takemoto, Ken Hattori, Masaaki Someta, Azusa N. Hattori, Hidekazu Tanaka, Kosuke Kurushima, Yuji Otsuka and Hiroshi Daimon

1. Instrument broadening.

The broadening arises from two factors: the incident X-ray character and the X-ray detection geometry. As shown in Fig. S1, the incident X-ray beam to the sample had a wave number of Q_α (4.075 Å^{-1}, where we assume $\omega = 2\theta = 0$ in Eq. 1 and Fig. 3 for simplicity) with a line width of ΔQ_α reflecting the longitudinal coherence length and the divergence angle of $\Delta\theta_{in}$ reflecting the transverse coherence length. In real space, the divergence induces incident beams 0-1, 0-4, and 0-5 in Fig. S1(a). In wave-number space, these correspond to incident vectors K_{in} from 0 to 1, 4, and 5 on the Ewald sphere of radius Q_α in Fig. S1(b). ΔQ_α results in the Ewald sphere width, corresponding to incident vectors 0-2 and 0-3.

The zero-dimensional (0D) X-ray detector with the slit acceptance angle of $\Delta 2\theta\chi$ was located a distance of 285 mm from the sample (i.e., the acceptance target length of $\lesssim$2.5 mm. In our X-ray condition, the irradiated area was $\simeq$11 mm in length and 2 mm in width. Since the whole acceptance region is covered by the irradiated area, outgoing X-ray beams 0-6, 0-9*, and 0-10* can be detected, as shown in Fig. S1(a). When the rotation of the detector ($2\theta\chi$ scan) and sample (ϕ scan), the slit also reduces the divergence between beams 0-9 and 0-10 in Fig. S1(a). Note that beams 0-9* and 0-9 are the same outgoing vector K_{out} in wave-number space, Fig. S1(b).

In reciprocal space as shown in Fig. S1(c), scattering vectors 4-9, 2-8, 5-10, and 3-7 induce mostly ellipsoidal broadening with Q_r and Q_φ axes around center scattering-vector 1-6. The broadening along Q_r (Q_φ) axes can be described as the components of (i) the longitudinal-coherence part as $\simeq\Delta Q_\alpha \sin\theta\chi$ ($2\Delta Q_\alpha \cos\theta\chi$) corresponding to scattering vectors 2-8 and 3-7, (ii) the transverse-coherence part as $\simeq Q_\alpha \Delta\theta_{in} \cos\theta\chi$ ($Q_\alpha \Delta\theta_{in} \sin\theta\chi$) corresponding to 4-6 and 5-6, (iii) the acceptance angle part as $\simeq Q_\alpha \Delta 2\theta\chi \cos\theta\chi$ ($Q_\alpha \Delta 2\theta\chi \sin\theta\chi$) corresponding to 1-9 and 1-10, and (iv) the rotation part as $\simeq 2Q_\alpha \cos\theta\chi\, \Delta\theta\chi$ ($2Q_\alpha \sin\theta\chi\, \Delta 2\theta\chi$) being $\frac{dQ_r}{d\theta\chi}\Delta\theta\chi$ ($Q_r \Delta\phi$) where $Q_r = 2Q_\alpha \sin\theta\chi$. When we treat Gaussian form, the square of instrument broadening σ_{inst-r} ($\sigma_{inst-\varphi}$) is the sum of the square of each component in (i)-(iv).

Measured 2D RSMs for Si 220, $\bar{2}20$, and 040 reflections are displayed in Figs. S2(a), S2(b), and S2(c), respectively. We can confirm ellipsoidal broadenings elongated to the radial directions: $\overrightarrow{Q_x}$ for 220, $\overrightarrow{Q_y}$ for $\bar{2}20$,and $\overrightarrow{Q_x} + \overrightarrow{Q_y}$ for 040, where σ_{inst-r} along Q_r is similar, while $\sigma_{inst-\varphi}$along Q_φ increases with Q_r. Table S1 shows measured σ_{inst-r} and $\sigma_{inst-\varphi}$ with $2\theta\chi_0$ for Si $220/\bar{2}20$ and 040 reflections. Using these values, we optimized ΔQ_α ($\simeq$0.007 Å^{-1}) corresponding to $\simeq$600 Å in longitudinal coherence, $\Delta\theta_{in}$ ($\simeq$0.47 °) corresponding to $\simeq$200 Å in transverse coherence, and $\Delta 2\theta\chi$ ($\simeq$0.25°). These lead to σ_{inst-r} ($\sigma_{inst-\varphi}$) of approximately 0.0182 Å^{-1} (0.0087 Å^{-1}), 0.0179 Å^{-1} (0.0094 Å^{-1}), and 0.0116 Å^{-1} (0.0174 Å^{-1}) for β-$FeSi_2$ 041, $042/02\bar{4}$, and $082/028$ reflections.

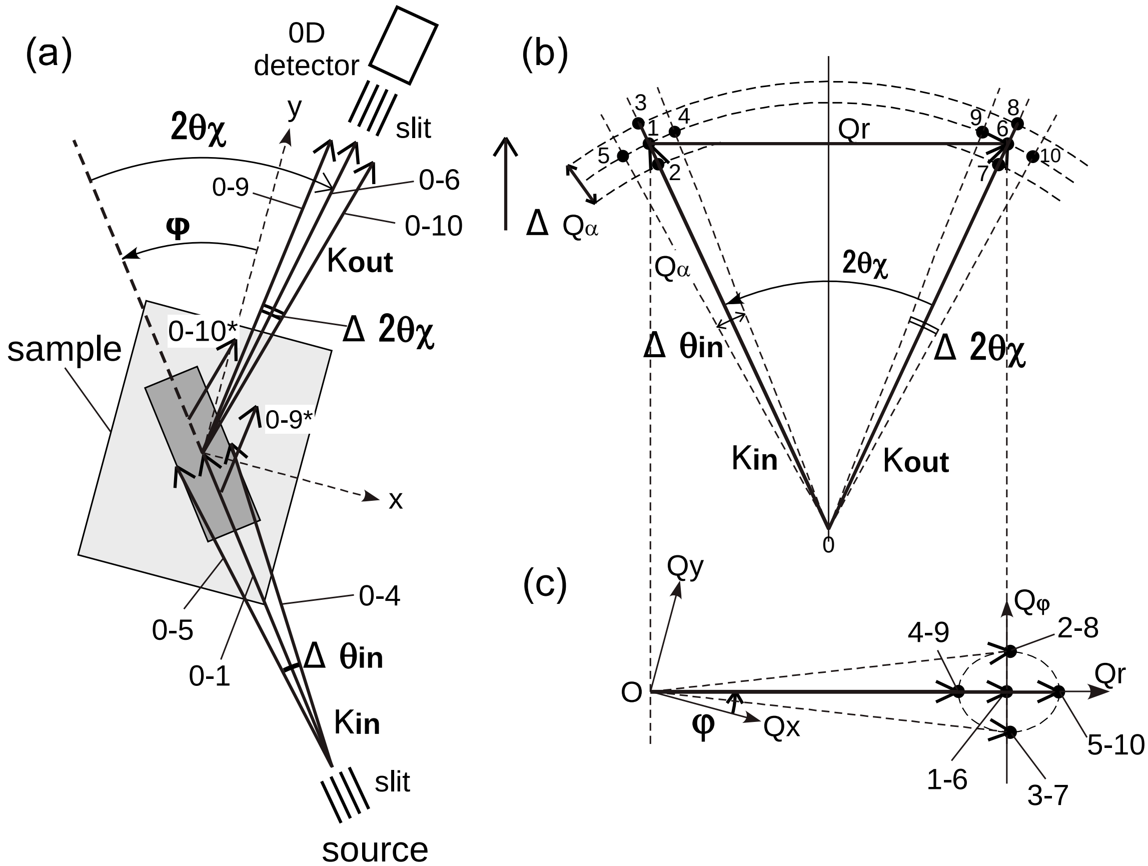

Fig. S1. Top-view schematics of X-ray diffraction in (a) real space, (b) Ewald-sphere picture, and (c) reciprocal space, when $\omega = 2\theta = 0$ in Fig. 3. K_{in} and K_{out} are the incident and diffracted X-ray vectors, with the divergence angle $\Delta\theta_{in}$ (inducing the transverse coherence) from the source and the acceptance angle $\Delta 2\theta\chi$ to the detector, respectively. The X-ray with a pair of numbers (e.g., 0-1) in (a) corresponds to the vector terminated with the same pair in (b). The Ewald radius of Q_α ($= |K_{in}| = |K_{out}|$) in (b) has the width of ΔQ_α inducing the longitudinal coherence. The scattering vector $Q_r = K_{out} - K_{in}$ in (b) is the basis of the reciprocal space map of (c) in the kinematical theory. Thus in (c), the scattering vectors (e.g., 5-10), around vector 1-6 corresponding to the peak center, contribute the instrument broadening.

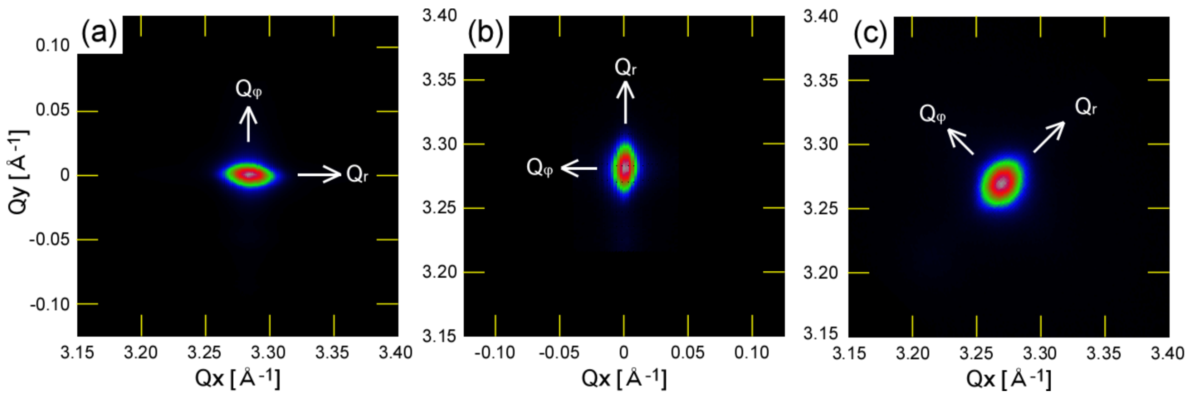

Fig. S2. 2D RSMs of Si reflection (a) 220, (b) $\bar{2}20$, and (c) 040.

Table S1. Diffraction angle $2\theta\chi_0$, instrumental broadenings σ_{inst-r} in r direction and $\sigma_{inst-\varphi}$ in φ direction for Si reflections.

Reflection	$2\theta\chi_0$ [°]	σ_{inst-r} [Å^{-1}]	$\sigma_{inst-\varphi}$ [Å^{-1}]
Si 220/$\bar{2}20$	47.34	0.018	0.009
Si 040	69.20	0.017	0.012

2. Analysis procedures

All data analyses were performed by homemade programs. The conversion from XRD results to 2D RSM in Eqs. 1 and 2 leads to intensities as a function of certain Q_x and Q_y sets. The experimental 2D RSMs in Figs. 4(a), 4(b), 4(i), and 4(j) with a step (pixel) of 0.0005 Å^{-1} were obtained by an interpolation from the Q_x and Q_y sets, using macro programs in the Image J application (https://imagej.nih.gov/ij/).

In the Gaussian fit, a program in the Mathematica application (https://www.wolfram.com) loaded the experimental 2D-RSMs, and minimized the residual from Gaussian functions at fixed ϵ and D according to Eqs. 7 and 8, using a *FindMinimum* command with an *InteriorPoint* algorism. The calculation resulted in I_{bg}, I_{peak}, and the residual value as displayed in Fig. 7, R maps. Since the number of unknown parameters are restricted to a few, and monitored convergence-process was smooth, the results are global minimum as indicated by a "monotonic" function of ϵ and D in Fig. 7. The calculation time was several sec per condition of fixed ϵ and D using a single processor.

In the Laue fit, similar programs in Mathematica was used for the calculations in Eqs. 9-13: (i) setting arbitrary unit-positions with ϵ_b, ϵ_c, N_b, and N_c (Eq. 9), (ii) the evaluation of L_A as a function of k_x and k_y with 0.001 $Å^{-1}$ step (Eq. 9), (iii) the convolution of L_A to LC_A with the integration by k_x and k_y with 0.001 $Å^{-1}$ step within the 3σ region (Eqs. 10-11), and (iv) the evaluation of the residual value (Fig. 8(a)) at fixed ϵ_b and ϵ_c (Eqs. 12-13), using the *FindMinimum* command which led to a global minimum. The calculation time in process (iv) was about 20 sec per condition. The first convolution-forming in process (iii) required about 8 hours but sequential convolutions required 5 min per condition. This will be improved using by fast convolution methods. The other calculation times were negligible.

For the inhomogeneous strain calculation in Eq. 14, the *FindMinimum* command was also used. Although the number of unknown parameters were over 360, it should be close to the global minimum because initial values in parameters did not affect the results in a few searching calculations. The calculation time was over 100 hours. Some calculations were performed in parallel using multiple processing systems in NAIST.

3. 2D Laue fit for inequivalent and homogeneous system

The residual map as a function of ϵ_b and ϵ_c for $N = N_b = N_c = 20$ ($D \simeq 160$ Å) is shown in Fig. S3; R_{min} is 0.18 at $\epsilon_b = 0.0\%$ and $\epsilon_c = -0.3\%$. This is larger than $R_{min} = 0.10$ for $N = 30$ ($D \simeq 230$ Å) in Fig. 8(a).

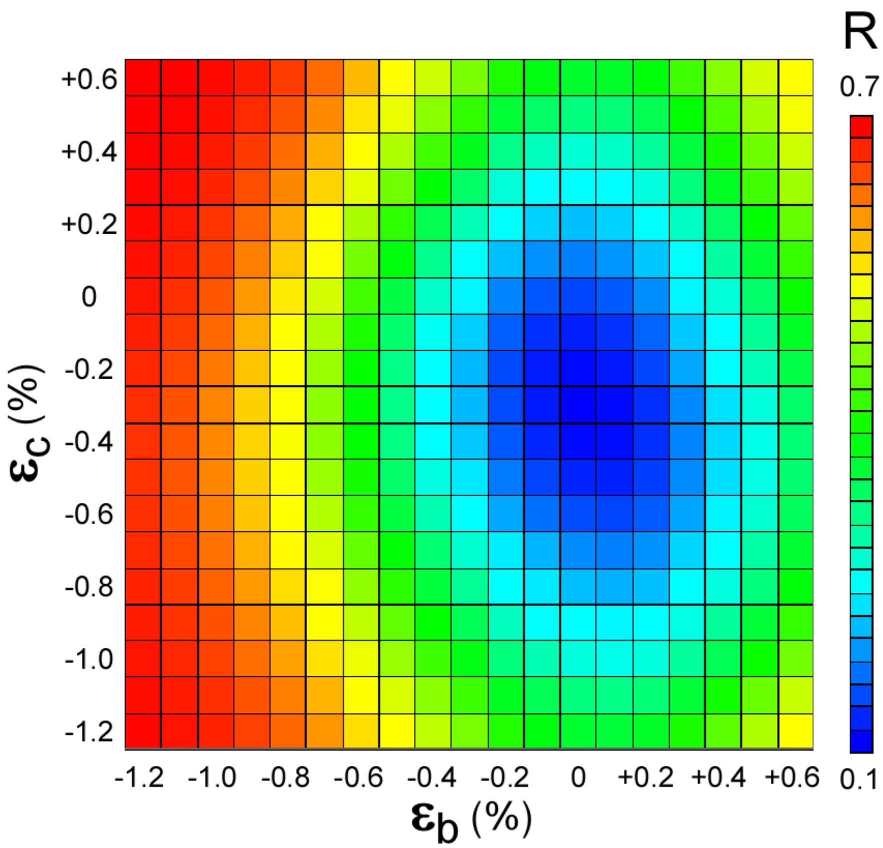

Fig. S3. Residual map as a function of inequivalent strains ϵ_b and ϵ_c along b and c axes, respectively, at $D \simeq 160$ Å ($N = 20$) under the homogeneous strain. $R_{min}$is 0.18 at $\epsilon_b = 0.0\%$ and $\epsilon_c = -0.0\%$.